Seafloor sediment thickness beneath the VoiLA broad-band ocean-bottom seismometer deployment in the Lesser Antilles from *P*-to-*S* delay times

Ben Chichester [1] Catherine Rychert,[1] Nicholas Harmon [1] Robert Allen,[2] Jenny Collier [2] Tim Henstock[1] and Andreas Rietbrock[3]

[1]*National Oceanography Centre Southampton, Ocean and Earth Sciences, University of Southampton, Southampton, UK. E-mail:* ben.chichester@southampton.ac.uk
[2]*Imperial College London, London, UK*
[3]*Karlsruhe Institute of Technology, Karlsruhe, Germany*

SUMMARY

Broad-band ocean-bottom seismometer (OBS) deployments present an opportunity to investigate the seafloor sediment thickness, which is important for constraining sediment deposition, and is also useful for subsequent seismological analyses. The Volatile Recycling in the Lesser Antilles (VoiLA) project deployed 34 OBSs over the island arc, fore- and backarc of the Lesser Antilles subduction zone for 15 months from 2016 to 2017. Using the amplitudes and delay times of *P*-to-*S* (*Ps*) scattered waves from the conversion of teleseismic earthquake *P* waves at the crust–sediment boundary and pre-existing relationships developed for Cascadia, we estimate sediment thickness beneath each OBS. The delay times of the *Ps* phases vary from 0.20 ± 0.06 to 3.55 ± 0.70 s, generally increasing from north to south. Using a single-sediment and single-crystalline crust earth model in each case, we satisfactorily model the observations of eight OBSs. At these stations we find sediment thicknesses range from 0.43 ± 0.45 to 5.49 ± 3.23 km. To match the observations of nine other OBSs, layered sediment and variable thickness crust is required in the earth model to account for wave interference effects on the observed arrivals. We perform an inversion with a two-layer sediment and a single-layer crystalline crust in these locations finding overall sediment thicknesses of 1.75 km (confidence region: 1.45–2.02 km) to 7.93 km (confidence region: 6.32–11.05 km), generally thinner than the initial estimates based on the pre-existing relationships. We find agreement between our modelled velocity structure and the velocity structure determined from the VoiLA active-source seismic refraction experiment at the three common locations. Using the *Ps* values and estimates from the VoiLA refraction experiment, we provide an adjusted relationship between delay time and sediment equations for the Lesser Antilles. Our new relationship is $H = 1.42\mathrm{d}t^{1.44}$, where H is sediment thickness in kilometres and dt is mean observed *Ps* delay time in seconds, which may be of use in other subduction zone settings with thick seafloor sediments.

Key words: Body waves; Wave scattering and diffraction; Backarc basin processes; Crustal structure; Sedimentary basin processes.

1 INTRODUCTION

Ocean-bottom seismometer (OBS) deployments present the opportunity for, and necessitate, determining the sediment thickness beneath each instrument. The impedance contrast at the crust–sediment boundary produces a *P*- to *S*-wave conversion (*Ps*) upon the arrival of a teleseismic earthquake. The delay time between the arrival of the parent *P* wave of the earthquake and the converted daughter *S* wave can then be used to estimate the thickness of the sediment, such as demonstrated at the East Pacific Rise (Harmon *et al.* 2007), in Cascadia (Rychert *et al.* 2018) and the Mid-Atlantic Ridge (Agius *et al.* 2018) where relationships with plate age and sedimentation rates are also observed. Characterization of the sediment package is important for seismological analysis of data recorded on the OBSs, such as for rotation into theoretical *P* and *S* components and for receiver function migration models (Rychert *et al.* 2018).

These constraints are also important for understanding regional sediment deposition and sediment material properties.

The VoiLA (Volatile Recycling in the Lesser Antilles) OBS deployment (see map in Fig. 1) represents an opportunity to expand and tighten constraints from previous active source reflection and refraction work (Christeson *et al.* 2008; Aitken *et al.* 2011; Allen *et al.* 2019) that suggest that ocean sediment thickness and type vary significantly over the Lesser Antilles. The sediment package is thick in the backarc of the subduction zone, particularly in the Grenada Basin that receives most of the arc's volcanogenic sedimentation via gravity flows based on seafloor coring and island field observations (Sigurdsson *et al.* 1980). Thickest is the sediment in the forearc due to its proximity to the Orinoco River delta in the south, similar gravity flows filling the Tobago Trough, and the pelagic and fluvial sediment being scraped from the subducting Atlantic plate forming the Barbados accretionary prism according to a plethora of various geophysical and coring analyses (Mann 1999; Picard *et al.* 2006). Sediment thickness reaches up to 15 km in the Grenada Basin and Tobago Trough, based on interpretation of refraction and reflection data collected along the BOLIVAR seismic line BOL30 (Christeson *et al.* 2008; Aitken *et al.* 2011) that was roughly 10 km further south than the southern-most VoiLA OBSs. Sediment thickness on the arc platform is relatively thin, typically less than 2 km thick (Speed 1993).

Here we estimate the seafloor sediment thickness beneath each OBS in the VoiLA deployment that were located on the arc, back- and forearc of the subduction zone. By using prior velocity–thickness relationships derived from active-source studies (Nafe & Drake 1957) and Rayleigh wave admittance inversion studies (Ruan *et al.* 2014), we initially translate the *Ps* delay times to estimates of the sediment thickness at each OBS. Next, we attempt to validate these estimated properties at each OBS by computing synthetic seismograms and comparing the amplitudes and delay times of the conversions to those in the data. Finally, we perform an inversion allowing a more complex, though likely realistic structure, that includes two sediment layers and a crystalline basement. New estimates and benchmarking to the VoiLA refraction experiment (Allen *et al.* 2019) allow us to propose a new relationship between observed *Ps* delay time and sediment thickness in the Lesser Antilles.

2 METHOD

2.1. Data and picking delay times

The National Environmental Research Council (NERC) of the United Kingdom-funded VoiLA project included an array of 34 four-component broad-band OBSs deployed for 15 months from February 2016 to May 2017, consisting of 24 German instrument pool for amphibian seismology (DEPAS) instruments and 10 Scripps Institute of Oceanography, USA (SIO) instruments. All instruments were recovered; however, two stations only began recording after recovery, leaving 32 usable broad-band OBSs distributed around the Lesser Antillean islands.

The horizontal components of the seismic stations are orientated by Rayleigh-wave polarization using the Doran-Laske-Orientation-Python (DLOPy) code (Doran & Laske 2017), and corrections for tilt and compliance noise are applied (Crawford & Webb 2000; Bell *et al.* 2015a). The *Ps* delay times are determined from the radial and vertical components of teleseismic earthquake arrivals limited to 25° to 90° epicentral distances. The waveforms are filtered

from 0.05 to 2.00 Hz, and a time window encompassing the first *P*-wave arrival on the vertical component and the subsequent arrival of the conversion on the radial component is manually picked by inspection. A time window is only picked if both arrivals are clear. Within the picked time window, the time and amplitude of both peaks are automatically determined, providing a peak-to-peak delay time and amplitude ratio for each event–station pair. This results in 302 event–station pairs using 30 unique earthquakes (inset in Fig. 1).

2.2 Initial estimate of sediment thickness using pre-existing relationships

To estimate sediment thickness beneath each station, we use the equation:

$$dt = h \left(\sqrt{\frac{1}{V_S^2} - u^2} - \sqrt{\frac{1}{V_P^2} - u^2} \right), \tag{1}$$

where dt is the *Ps* delay time in s; h is the total sediment thickness in km; V_S and V_P are average *S*- and *P*-wave velocities of the sediment in $km\,s^{-1}$ between the surface and h; and u is the ray parameter in $s\,km^{-1}$.

V_P as a function of depth in km, z, is estimated using the linear relationship for deep water empirically derived by Nafe & Drake (1957),

$$V_P(z) = 0.43z + 1.83. \tag{2}$$

We determine V_S as a function of depth using the function of Ruan *et al.* (2014):

$$V_S(z) = \left(az^2 + bz + cV_{S(0)} \right) / (z + c), \tag{3}$$

where $V_{S(0)}$ is the sediment shear velocity at the seafloor; and $a = 0.15608$, $b = 1.2198$ and $c = 0.49473$ are constant model parameters determined by inverting Rayleigh wave admittance functions for the sediment shear velocity–depth profiles beneath OBSs that were deployed on the Juan de Fuca plate (Ruan *et al.* 2014; Bell *et al.* 2015b). Eq. (3) is chosen by Ruan *et al.* (2014) and Bell *et al.* (2015b) to account for the rapid increase in shear velocity with depth at shallow sediment depths and a more gradual increase at greater sediment depths, and the relationship was only confirmed for sediment up to 1 km thick. $V_{S(0)}$ is assumed to be 100 ms^{-1} based upon measurements in water-saturated sand (Hamilton 1979). In order to model a single layer of sediment with these continuous functions of depth, from eqs (2) and (3) we take the average velocities, V_P and V_S, from depths of $z = 0$ to $z = h$ for use in eq. (1).

2.3 Synthetic tests of *Ps/P* amplitude ratios versus slowness

We perform synthetic waveform forward modelling in an attempt to verify the previously existing relationships, outlined above, that we use to inform the relationship between delay time and sediment thickness. We compute 1-D reflectivity synthetic waveforms (Shearer & Orcutt 1987) with simple four-layer 1-D seismic velocity–depth profiles using sediment values initially based on the derived values from those relationships. Waveforms are computed using the ray parameter of the earthquake of each observed event–station pair. The four layers in the 1-D profiles are: the water column using the water depth of each OBS, sediment, crust of thickness determined by subtracting the estimated sediment thickness from the crustal thickness obtained from CRUST1.0 (Laske *et al.* 2013), and
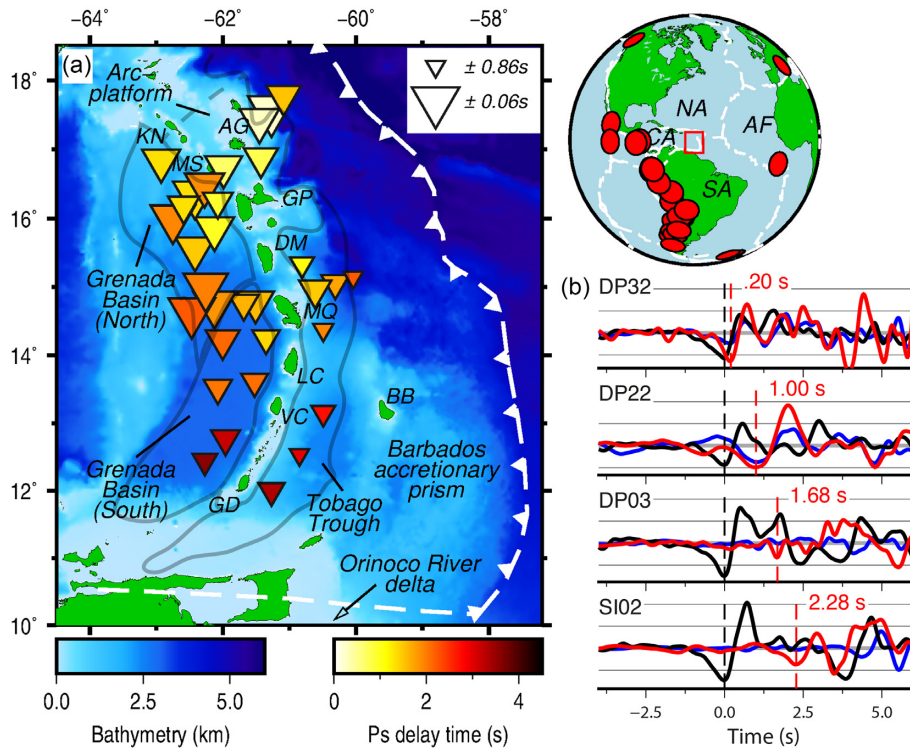
Figure 1. (a) Bathymetry of the Lesser Antilles region and average *P*-to-*S* (*Ps*) delay times at each ocean-bottom seismometer (OBS) of the VoiLA deployment (inverted triangles). Size of inverted triangle describes level of observation uncertainty. Grey lines delineate the different features used to group OBSs, based on Picard *et al.* (2006). Island labels in main figure are: KN, St. Kitts and Nevis; AG, Antigua and Barbuda; MS, Monserrat; GP, Guadeloupe; DM, Dominica; MQ, Martinique; LC, St. Lucia; VC, St. Vincent and the Grenadines; GD, Grenada; BB, Barbados. Bathymetry from ETOPO1 (Amante & Eakins 2009). Top right-hand panel: reference map including study area, red box; earthquakes used, red circles; plate boundaries, white dashed lines (Bird 2003); and relevant tectonic plates (NA, North American; SA, South American; CA, Caribbean; AF, African). (b) Example *P*-wave arrivals and subsequent *Ps* phases on four OBSs, from the same earthquake (21/02/2017 14:09 UTC, M$_w$ 6.5). The waveforms are the vertical (black), radial (red) and transverse (blue) components. Black and red dashed lines are the *P*-wave arrival and the converted *Ps* arrival, respectively. The figure was made using Generic Mapping Tools (Wessel *et al.* 2013).

an underlying mantle. The reason for using CRUST1.0 and not a crustal thickness of ~7 km common across most ocean lithosphere is that oceanic crust around volcanically active ocean islands is commonly thicker than normal ocean crust (Leahy *et al.* 2010). The crust in the Lesser Antilles may also be affected by the Caribbean large igneous province. Densities used in the model are 1.03 g cm^{-3} for the water column; 2.0 g cm^{-3} for the sediment; 2.8 g cm^{-3} for the crystalline crust; and 3.3 g cm^{-3} for the mantle. Compressional and shear velocities of layers are, respectively, 1.5 and 0 km s^{-1} for the water column; 6.8 and 3.82 km s^{-1} for the crystalline crust; and 8.2 and 4.5 km s^{-1} for the mantle. For the water column, we actually use a very low, non-zero shear velocity (0.00001 km s^{-1}) due to numerical limitations of the reflectivity code (Müller 1985). The ratio of the first peak amplitudes of the radial and vertical components (or the converted and parent phases, respectively) and the delay time are measured in each case to compare to observations.

2.4 Error

Uncertainties for delay times are defined by one standard deviation of all observed delay times at each individual station, and we do not consider individual measurement error. Uncertainties for sediment thickness of each station are propagated from the delay time errors using eqs (1), (2) and (3).

The acceptable threshold for synthetic fits of amplitude ratios is determined by the scatter of the observed amplitude ratios of

the entire OBS deployment. In other words, we calculate one standard deviation from the regressed line when plotted against slowness for each OBS, then average these individual standard deviations over the array, finding a value of ±0.26. This error in the data is represented by the grey error region above and below the regressed, dash–dotted line in the top panels of Figs 2, 4 and 5. A model is considered a fit when the synthetic values of amplitude ratio versus slowness falls within this acceptable error region.

2.5 Inversion for a two-layer sediment package

In a final approach, we invert the amplitude ratios and delay times in the data using synthetic seismograms that we create assuming a two-layer sediment and a single-layered crystalline crust. The amplitudes of the daughter and converted peaks and delay times are picked from each synthetic waveform and compared to those in the data, and the synthetic waveforms are recomputed on each iteration of the inversion. The inversion uses a non-linear optimization based on the interior-point method implemented in MATLAB (Waltz *et al.* 2006). The objective function, *F*, which we minimize for each station separately, is the sum of the normalized mean squared error of the predicted amplitude ratio from the observed amplitude ratio, summed to that of delay time. The observational error of each point from the mean (the respective dotted lines of delay time and amplitude ratio in Figs 2, 4 and 5) at each station is used for normalization,
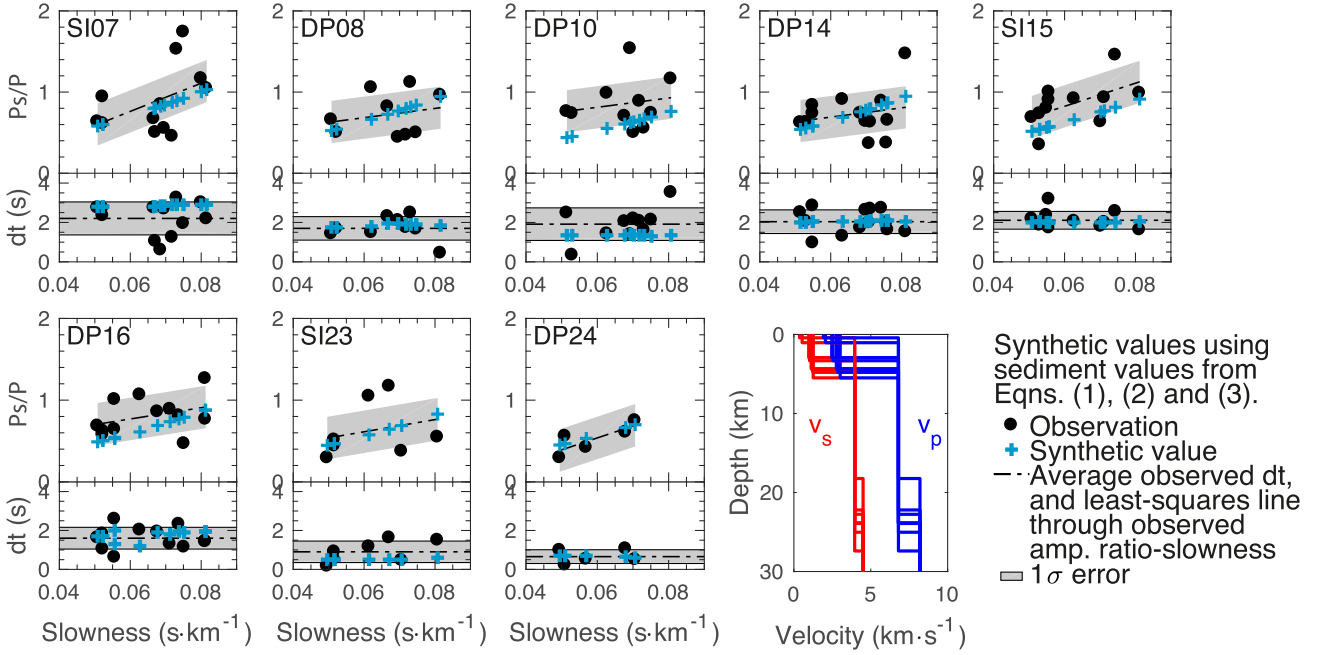
Figure 2. Initial synthetic modelling results of ocean-bottom seismometers (OBS) that generate synthetic fits to the observed values of *Ps/P* amplitude ratios (upper panels) and delay times (lower panels), using an earth model that features sediment properties estimated by eqs (1), (2) and (3) in text and a crust based on CRUST1.0. Black dots, observed data; blue crosses, synthetic values. The error bar for the amplitude ratio represents the average observation standard deviation over all OBSs (± 0.26), described in text. The error bar for the delay time is the standard deviation on each corresponding OBS. The velocity-depth profile presents the structure used in the synthetic model of each station, showing similar crustal structure that varies only based on CRUST1.0 and the estimated sediment thickness—blue, V_P; red, V_S.

ε_{A_i} and ε_{dt_i}:

$$F = \sum_i^N \left[\left(\frac{A_i^{obs} - A_i^{pred}}{\varepsilon_{A_i}} \right)^2 \right] + \sum_i^N \left[\left(\frac{dt_i^{obs} - dt_i^{pred}}{\varepsilon_{dt_i}} \right)^2 \right], \quad (4)$$

where N is the number of observations for each respective station; A^{obs}_i and dt^{obs}_i are the observed amplitude ratios and delay times, respectively; and A^{pred}_i and dt^{pred}_i are the synthetic values of the predicted model from each iteration of the inversion. Our inversion parameters are thickness, V_P, and V_P/V_S for each layer, comprising nine unknowns. We optimize the solution with the following constraints: the velocity must increase with depth; V_P must be between 1.5 and 6.8 km s^{-1} for the two sediment layers and 3.5–7.9 kms^{-1} in the underlying crustal layer; and V_P/V_S must be between 1.72 and 3.0 for the two sediment layers and 1.72–1.9 in the crustal layer. The optimization uses the gradient in the objective function with respect to each model parameter and the approximate Hessian to iteratively inform and update the model. Optimizations typically converge within 10–20 iterations. The problem we are solving is non-linear, and involves nine parameters, so estimating uncertainty in all of the parameters including covariance is not straight forward without a full grid search. We are primarily interested in sediment thickness, so we examine the error bounds on these parameters by searching over sediment thickness for both layers, using a line search for each thickness parameter individually, and a grid search for both thickness parameters simultaneously. We search over the 0–12 km thickness and accept models that produce delay times and amplitude ratios that both fall within their respective observational error regions of the data (grey regions in Figs 2, 4 and 5). For the line search, each sediment layer is treated independently, and the other eight parameters to the one being searched over are kept at the optimal value found in the inversion. The minimum and maximum

sum of these accepted sediment layer thicknesses are used as the error bounds for the inversion result of sediment thickness beneath each station (Fig. 6). This approach does not take the covariance of the thickness of the two sediment layers into account. However, the 2-D grid-search, which we perform to explore the effect that covariance imposes on the error bounds, only produces notably larger error bounds at stations located in the southern back- and forearc basins. This is likely due to the complexity of the Earth structure in this region of the study. Error bounds in Fig. 6 do not reflect the covariance, but we do report the error bounds of both methods in Table 2.

3 RESULTS

3.1 Delay times and initial sediment thickness estimates

Station averages of *Ps* delay times generally increase from north to south (Fig. 1a). Average station delay times vary from 0.20 ± 0.06 s (OBS DP32), to 3.55 ± 0.70 s (OBS DP01)—these are presented in Table 1, along with equated initial estimates of sediment thickness, our inversion results, and VoiLA refraction results where available. The delay times generally vary according to expectations based on tectonics and proximity to the continental shelf. In the north, OBSs placed on the present arc-platform, or on the old arc-platform that formed before the island arc underwent bifurcation (D. E. Bird *et al.* 1999), exhibit average delay times ranging from 0.20 ± 0.06 to 1.89 ± 0.29 s. In the backarc, mostly comprising of the Grenada Basin, average delay times generally increase from north to south from 0.99 ± 0.30 to 3.55 ± 0.70 s. Similarly, on the forearc, delay times generally increase towards the south as the OBSs become proximal to the Barbados accretionary prism and the southern To-bago Trough from 1.53 ± 0.42 to 3.32 ± 0.66 s.
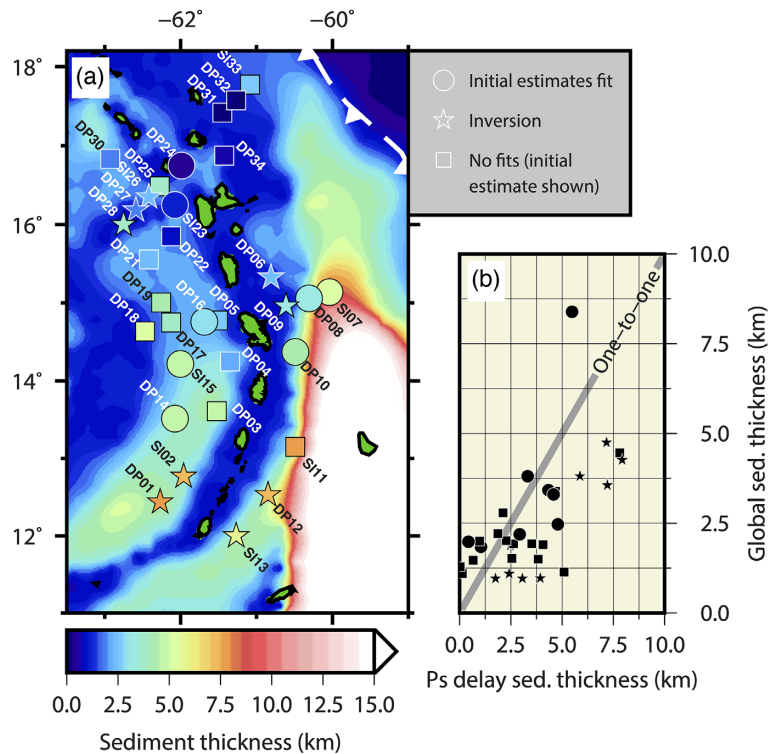
Figure 3. Estimated sediment thickness from *P*-to-*S* delay times compared to the global sediment thickness model of Straume *et al.* (2019). (*a*) Colour scale is shared by the background (global model) and the coloured shapes. Circles: ocean-bottom seismometers (OBS) on which initially estimated sediment properties based upon delay time and eqs (1), (2) and (3) in text allowed a synthetic fit to the data (Fig. 2). Sediment thickness is the average estimate at each OBS. Stars: OBSs on which an inversion for sediment and crustal structure produced a new synthetically fitting model (Fig. 5). Squares: OBSs on which neither method generates a synthetic fit to the observations—the thickness shown is the initial estimate based on delay time and eqs (1), (2),and (3) in text. Dashed white front indicates the subduction trench (Bird 2003). White and black OBS labels and shape borders differ for visual distinction. (b) Graphical comparison. Shapes follow the key in (a). The figure was made using Generic Mapping Tools (Wessel *et al.* 2013).

The generated amplitude ratio–slowness curves from the 1-D synthetics that we compute generally match the trend of increasing amplitude ratio with horizontal slowness on each OBS. For those with a discernable trend, using the initial estimates estimated from eqs (1), (2) and (3), the synthetically computed parent and converted phase for 8 out of 32 of the OBSs generate amplitude ratios that fit the observed values, while simultaneously exhibiting delay times that fall within the observed error in delay time. The observed delay times and amplitude ratios and the synthetic results for these stations are presented in Fig. 2. Sediment thickness estimated this way ranges from 0.43 ± 0.45 to 5.49 ± 3.23 km (Fig. 3, circles).

The remaining 24 out of 32 stations either: (1) do not exhibit observations that we are able to synthetically fit when using the initial estimates of sediment properties in the simple four-layer 1-D model (the synthetic amplitude ratio–slowness curve for the corresponding station is not within the previously determined acceptable error limit on amplitude ratio, and/or the synthetic delay time is not within the observed error of the corresponding station) or (2) do not exhibit observed amplitude ratio–slowness trends that we can fit (i.e. there is too much scatter). The observed delay times and amplitude ratios and those of the attempted synthetics for these stations are presented in Fig. 4, with those stations that do not exhibit a modellable trend labeled in red. Sediment thickness estimated on these stations ranges from 0.03 ± 0.01 to 12.53 ± 4.43 km, which is also the entire range found using the observed delay times and eqs (1), (2) and (3), and indicates that sediment thickness is not the cause of the difficulty we encounter in modelling many of the stations.

3.2 Inversion

We perform the inversion for 17 OBSs on which our initial estimates of sediment properties based on eqs (1), (2) and (3) did not produce fitting synthetics, and which also have observational scatter exhibiting a clear trend, to search for new sediment and crystalline crustal properties that do fit the observed data. The inversion finds parameters that successfully fit the observed data on 9 of these 17 OBSs. We present the optimal Earth model for each successful station in Fig. 5, and sediment thicknesses compared to our initial estimates and VoiLA refraction results of Allen *et al.* (2019) in Fig. 6. Error estimates for the sediment thicknesses from the refraction profiles (Allen *et al.* 2019) beneath each OBS node are calculated using the program DMPLSTSQR in conjunction with RAYINVR (Zelt & Smith 1992). Calculation assumed a worst-case velocity uncertainty with a standard deviation of 0.25 kms^{-1} in all model layers.

On the arc-platform and in the northern Grenada Basin, the inversion generates sediment thicknesses that agree well with our initial estimates that are based on eqs (1), (2) and (3). OBS DP06 exhibits an inversion sediment thickness of 2.42 km (confidence region (CR): 1.42–2.51 km) compared to our initial estimate of 1.59 ± 1.63 km. When producing the synthetic for our initial estimate, the crystalline crustal thickness (the crustal portion beneath the sediment package) is 22.27 km, whereas the inversion converges on a crystalline crustal thickness of 6.97 km. In the northern Grenada Basin, OBSs SI26, DP27 and DP28 exhibit inversion sediment thicknesses of 2.48 km (CR: 2.46–2.52 km), 1.75 km (CR: 1.45–2.02 km) and 3.94 km (CR: 3.54–4.15 km), respectively, compared to our initial estimates
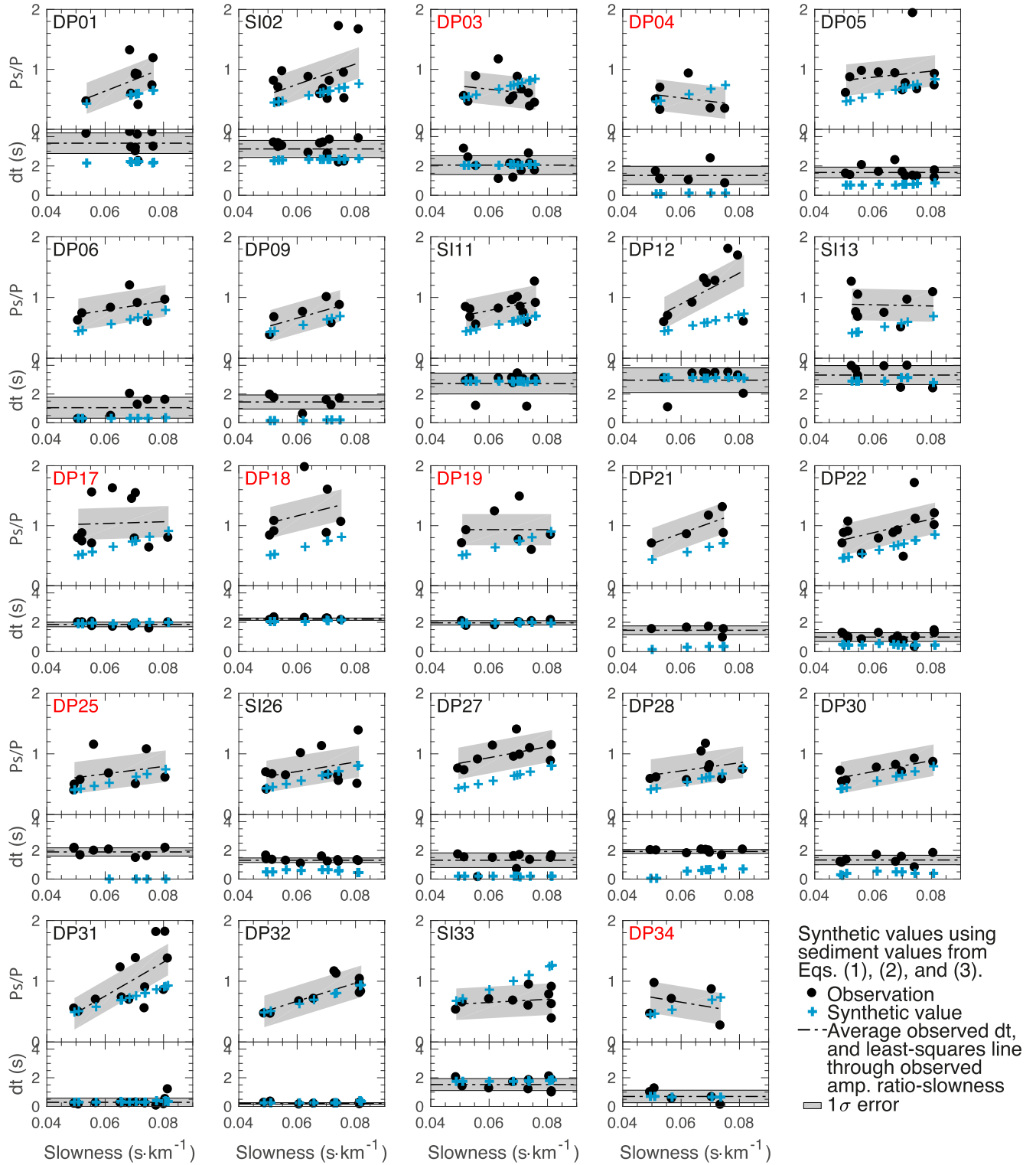
Figure 4. Initial synthetic modelling results of ocean-bottom seismometers (OBS) that do not generate acceptable synthetic fits to the observed *Ps/P* amplitude ratios (upper panels) or delay times (lower panels), or where there is too much scatter to fit (OBSs labelled in red). Black dots, observed data; blue crosses, synthetic values. Earth models used to generate synthetics feature sediment properties estimated from eqs (1), (2) and (3) in text and crust based on CRUST1.0. The error bar for the amplitude ratio represents the average observation standard deviation over all OBSs (±0.26), described in text. The error bar for the delay time is the standard deviation on each corresponding OBS.
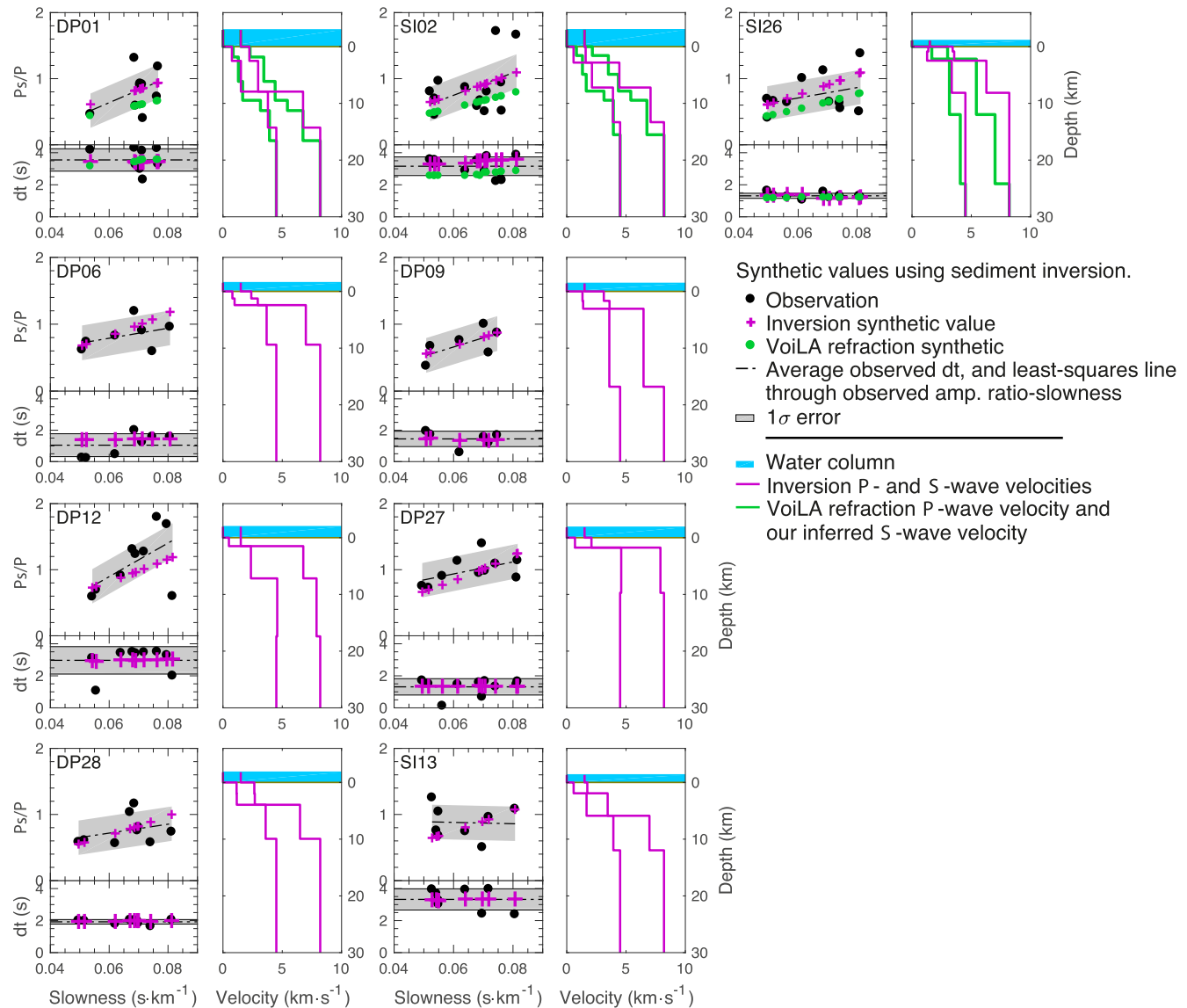
Figure 5. Inversion results of new sediment and crustal structure beneath ocean-bottom seismometers (OBS) that generate synthetic fits to the observed values of amplitude ratio and delay time. The top three plot pairs present OBSs that exhibit interpreted structure from the VoiLA refraction experiment (Allen *et al.* 2019) that we are able to successfully synthetically model by inferring a shear velocity (green), compared to the inversion results (magenta). The error bar for the amplitude ratio (top left of each OBS plot pair) represents the average observation standard deviation over all OBSs (± 0.26), described in text. The error bar for the delay time (bottom left of each OBS plot pair) is the standard deviation on each corresponding OBS. Blue regions above zero in the velocity–depth profiles (right of each OBS plot pair) represent the water column.

of 1.76 ± 0.51, 2.03 ± 1.07 and 3.91 ± 0.54 km. The inversion sediment thickness for OBS SI26 falls outside the error bounds from our initial estimate. When producing the synthetic for our initial estimate, the crystalline crustal thickness in each case is 20.45, 20.18 and 18.30 km, respectively, whereas the inversion converges on a crystalline crustal thickness of 5.66, 7.97 and 5.98 km.

In the Tobago Trough, OBSs DP09, DP12 and SI13 exhibit inversion sediment thicknesses of 3.06 km (CR: 2.71–4.08 km), 7.17 km (CR: 4.01–9.04 km) and 5.87 km (CR: 3.65–8.08 km), respectively, which are within the error bounds of our initial estimates of 2.38 ± 1.37, 9.14 ± 3.85 and 11.12 ± 3.89 km. The crystalline crustal thickness used when attempting to synthetically model our initial estimates are 23.92, 26.14 and 10.96 km, respectively, whereas the inversions converge on 13.75, 10.22 and 16.56 km.

In the southern Grenada Basin, OBSs DP01 and SI02 exhibit inversion sediment thicknesses of 7.93 km (CR: 6.32–11.05 km) and 7.21 km (CR: 2.82–7.80 km), respectively, which are within error bounds of our initial estimates of 12.53 ± 4.43 and 10.02 ± 3.18 km. The crystalline crustal thickness used when attempting to synthetically model the initial estimates are 9.01 and 12.07 km, respectively, whereas the inversions converge on 6.34 and 6.10 km.

4 DISCUSSION

Our results show sediment thickness varies by region, using the tectonic regionalization of Picard *et al.* (2006). The average sediment thickness we estimate for the arc platform is 1.43 km, which is thinner than any other region. The sediment here is likely much thinner than this value, as indicated by very low delay times observed
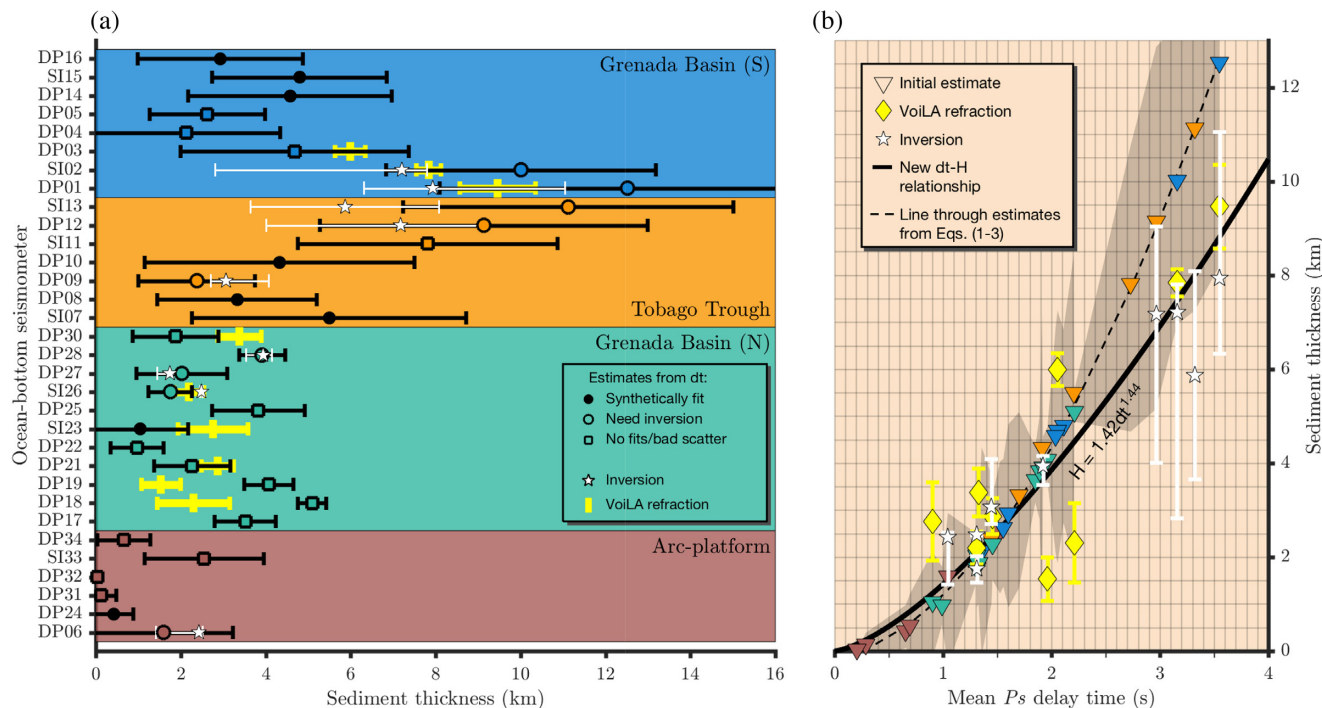
Figure 6. Comparison of different estimates of sediment thickness. (a) Regional, station-wise sediment thickness. Solid black circles, empty black circles and empty squares: average estimated sediment thickness according to *P*-to-*S* delay times and eqs (1), (2) and (3) in text, where error bars denote the standard deviation of this estimate on each station. White stars: optimal sediment thickness from inversions on each station, where error bars denote the range of sediment thickness around that optimal value where a synthetic fit to observed delay time and amplitude ratio is also determined. Yellow bars: sediment thickness determined by the VoiLA refraction experiment (Allen *et al.* 2019) beneath stations over which a cruise line traversed. (b) Comparison of mean observed delay times to our estimates of sediment thickness [inverted triangles, colour-coded to regions in (a)], those of the VoiLA refraction (yellow diamonds), and inversion results [white stars and same error bars as in (a)]. Dashed black line: polynomial fit to our estimates associated with relationships of Ruan *et al.* (2014) and Nafe & Drake (1957). Shaded grey region: one standard deviation of our estimated sediment thickness determined from delay time and the equations about each OBS. Solid, thick black line: our new proposed delay time–sediment thickness relationship based on the regressed power law through inversions, VoiLA refraction results, and initial estimates thinner than 1 km.

on OBSs DP31 and DP32 that we are unable to model. The next thinnest sedimentary province is the northern Grenada Basin with an average of 2.30 km. The Tobago Trough and southern Grenada Basin exhibit thicker average sediment thickness results of 4.87 and 5.49 km, respectively, with similar ranges that generally increase from north to south: 3.06 km (CR: 2.71–4.08 km) to 7.17 km (CR: 4.01–9.04 km) in the Tobago Trough and 2.93 ± 1.95 km to 7.93 km (CR: 6.32–11.05 km) in the southern Grenada Basin. The distribution of sediment thickness over the different regions reflects preferential sediment deposition into the fore- and backarc basins. The north-south trend of thickening sediments in the southern half of the study is due to increasing proximity to the South American continent and the Orinoco River delta.

The regional differences in sediment thickness in our results agree with regional variations reported by the global sediment thickness model (Straume *et al.* 2019)—that is much thicker in the back- and forearc basins, and thinner on the arc platform (Fig. 3). However, in the back- and forearc basins, we generally estimate thicker sediment packages than in the global compilation (Straume *et al.* 2019). In the Caribbean region, the global compilation (Straume *et al.* 2019) uses two-way travel times of various active-seismic profiles (Mascle *et al.* 1985; Udintsev 1994), which are up to 5 s in the Grenada Basin and Tobago Trough and indicate that a seismic velocity of ∼2 km s^{-1} was used. The drop-off in sediment thickness here compared to our estimates (Fig. 3b) may be explained by the fore- and backarc basins consisting of sediments that, on average, are seismically faster than

∼2 km s^{-1} (Aitken *et al.* 2011), or that the reflection seismic used in the global compilation may not have had the capacity to penetrate the entire sedimentary package. The two-way traveltimes used in the global compilation may be constraining interfaces between three main sedimentary layers that, based on abrupt changes in seismic signature in the basins, are interpreted to have been deposited from the Paleogene at the base of the sediment package to recent assemblages at the surface (Aitken *et al.* 2011, Allen *et al.* 2019). Furthermore, our successful inversions for OBSs DP01, SI02, DP12 and SI13 in the southern Grenada Basin and Tobago Trough demonstrate that multiple sediment layers are required to fit the observed data. Interpretation of multiple refractors along a VoiLA refraction line in the southern Grenada Basin also indicates multiple sediment layers (Allen *et al.* 2019), which we have modelled on OBSs DP01 and SI02 (Fig. 5).

Our best-fitting sediment thicknesses from the inversions are also generally consistent within error with those found by the VoiLA refraction experiment (Allen *et al.* 2019, DP01: inversion result 7.93 km (CR: 6.32–11.05 km) versus refraction result 9.46 ± 0.89 km; SI02: 7.21 km (CR: 2.82–7.80 km) versus 7.84 ± 0.29 km; and SI26: 2.48 km (CR: 2.46–2.52 km) versus (2.19 ± 0.35 km). Comparing the predicted velocity profiles to those of refraction in 1-D shows that our predicted structures are similar, despite the refraction model having more layers, owing to higher resolution. Adding more layers and parameters to our model to achieve a better fit is not justified given the frequency content and

Table 1. VoiLA OBSs, Number of events used, Average P-Pds delay time and standard error, Average sediment thickness based on eqs (1)–(3) and standard error, Inversion sediment thickness and VoiLA refraction sediment thickness (Allen *et al.* 2019).

Station	# Events	Av. d*t* (s)	Error (s)	Av. H (km)	Error (km)	Inversion H (km)	Refraction H (km)
DP01	9	3.55	0.70	12.53	4.43	**7.93**	**9.46**
SI02	13	3.16	0.58	10.02	3.18	**7.21**	**7.84**
DP03	11	2.06	0.64	4.68	2.68		5.99
DP04	6	1.36	0.62	2.12	2.22		
DP05	11	1.56	0.36	2.63	1.36	✗	
DP06	7	1.05	0.73	1.59	1.63	**2.42**	
SI07	12	2.20	0.84	**5.49**	3.23		
DP08	9	1.70	0.60	**3.32**	1.87		
DP09	6	1.45	0.49	2.38	1.37	**3.06**	
DP10	10	1.91	0.83	**4.33**	3.17		
SI11	13	2.73	0.73	7.81	3.05	✗	
DP12	9	2.97	0.86	9.14	3.85	**7.17**	
SI13	8	3.32	0.66	11.12	3.89	**5.87**	
DP14	13	2.04	0.60	**4.58**	2.40		
SI15	11	2.11	0.45	**4.79**	2.06		
DP16	12	1.60	0.56	**2.93**	1.95		
DP17	11	1.82	0.19	3.52	0.72		
DP18	7	2.21	0.08	5.10	0.34		2.30
DP19	7	1.96	0.15	4.07	0.58		1.53
DP21	5	1.46	0.30	2.27	0.90	✗	2.87
DP22	13	0.99	0.30	0.97	0.62	✗	
SI23	7	0.90	0.55	**1.04**	1.13		2.76
DP24	5	0.66	0.35	**0.43**	0.45		
DP25	8	1.89	0.29	3.83	1.09		
SI26	11	1.31	0.16	1.76	0.51	**2.48**	**2.19**
DP27	10	1.31	0.51	2.03	1.07	**1.75**	
DP28	9	1.92	0.14	3.91	0.54	**3.94**	
DP30	8	1.33	0.33	1.87	1.01	✗	3.38
DP31	13	0.29	0.28	0.13	0.35	✗	
DP32	10	0.20	0.06	0.03	0.01	✗	
SI33	10	1.53	0.42	2.55	1.41	✗	
DP34	5	0.77	0.43	0.66	0.63		

VoiLA: Volatile Recycling in the Lesser Antilles.
Sediment thicknesses in **bold** are values we have synthetically validated and place more confidence in.

Table 2. VoiLA OBSs with successful inversions, Inversion sediment thickness, Lower/Upper error bound from 1-D grid-search, Lower/Upper error bound from 2-D grid-search.

Station	Inversion H (km)	1-D Min. (km)	1-D Max. (km)	2-D Min. (km)	2-D Max. (km)
DP01	7.93	6.32	11.05	4.00	13.40
SI02	7.21	2.82	7.80	3.00	14.00
DP06	2.42	1.42	2.51	0.80	2.70
DP09	3.06	2.71	4.08	2.40	4.20
DP12	7.17	4.01	9.04	1.80	8.80
SI13	5.87	3.65	8.08	2.00	9.60
SI26	2.48	2.46	2.52	2.40	2.70
DP27	1.75	1.45	2.02	1.60	2.00
DP28	3.94	3.54	4.15	3.60	4.10

VoiLA: Volatile Recycling in the Lesser Antilles.

spatial resolution of our data. Sediment packages can be far more complex than resolvable by our data, including features such as unconformities and dipping layers (Aitken *et al.* 2011), or interactions between highly varying sediment types (Picard *et al.* 2006). Indeed, the coefficients in eq. (3) were developed for the sediments in Cascadia (Ruan *et al.* 2014; Bell *et al.* 2015b), whereas the sediments of the Lesser Antilles likely host a different mix of pelagic, volcanoclastic and terrigenous sediments, and one that also likely highly

varies geographically (Picard *et al.* 2006). Given the size of our error bars, and the added complexity we encountered with waveform interference from multiple layers of sediment and/or crust, we do not have the resolution to determine new coefficients independently. These complexities may be the cause of OBSs DP05, SI11, DP21, DP22 DP30, DP31, DP32 and SI33 exhibiting no fit to the data using our initial estimates of sediment properties nor our inversion for multiple layers.

The utility of using *Ps* phases is that one can potentially rapidly estimate sediment thickness and infer sediment properties from a relatively simple measurement. In addition, using both the amplitude and delay time of the *Ps* conversion as we have done here can ideally disambiguate trade-off between sediment velocity and thickness, given that the amplitude of converted phases are not sensitive to changes in density (Rychert *et al.* 2007). However, we find that in a region with complex geology and/or thick sediment as in the Lesser Antilles, a simple, singular sediment layer assumption could only satisfy data amplitude and delay times for a subset of stations. Only in eight cases (OBSs SI07, DP08, DP10, DP14, SI15, DP16, SI23 and DP24) the single sediment layer assumption works and are validated when we use preexisting relationships. Otherwise, inverse modelling with several sediment and crystalline crustal layers is required. Specifically, in order to model the *Ps* phases in most cases we need either a more complex crystalline

crustal structure in the north near the arc, or multiple sediment layers in the south, where sediments are significantly thicker. In the south (OBSs DP01, SI02, DP12 and SI13) our inversions allowing multiple layers produce sediment thicknesses that are on average 3.66 km thinner than our initial estimates that assume a single sediment layer, and are a better match to sediment thicknesses from VoiLA refraction (available beneath DP01 and SI02). This suggests that accounting for multiple sediment layers is important at least in the south. Our results agree well with expectations for a thick and layered sediment package in the south of the Grenada Basin, for instance from refraction and reflection (Aitken *et al.* 2011), and with a sub-sedimentary oceanic crust in the southern Grenada Basin based on refraction and gravity data (Boynton *et al.* 1979; Christeson *et al.* 2008; Allen *et al.* 2019) that is thin compared to CRUST1.0, which we use in initial modelling. In the north (OBSs SI26, DP27 and DP28), inverting for different crustal properties seems more important, as successful inversions find similar sediment structure to our initial estimates, but require a lower-crustal boundary at much shallower depths. This boundary likely reflects a mid-crustal discontinuity rather than the Moho, as subsedimentary crust in the northern Grenada Basin is thicker island arc crust, based on various geophysical and chronological data (Bouysse 1988), and is likely layered according to the VoiLA refraction experiment (Allen *et al.* 2019). The requirement for multiple layering when modelling the *Ps* phases here contrasts other regions where a single sediment layer is sufficient, such as on young oceanic lithosphere (e.g. Agius *et al.* 2018; Rychert *et al.* 2018). The locations where a single layer assumption works, which are in the centre of the arc (OBSs SI07, DP08, DP10, DP14, SI15 and DP16), likely correspond to places where the sediment package is not thick enough to develop observable internal layering and the crust is still relatively simple, thinner, oceanic crust, that is not significantly layered. Indeed, inversions on OBSs DP06 and DP09 are successful with thin sediment with small extents of layering and the imposed single-layered crystalline crust.

Combining our *Ps* derived sediment thicknesses and those from the VoiLA refraction experiment, we propose a new relationship between mean observed *Ps* delay time and sediment thickness in the Lesser Antilles to aid in rapid assessment of sediments beneath an OBS array. Even with complications such as multiple sediment layers and variable crystalline crustal properties the overall thickness and delay time are related upon inspection (Fig. 6b) and the relationship might be reasonably approximated by a power law of *Ps* delay time. We choose a power law form to account for sediment compaction with depth after Alibés *et al.* (1996). We determine the new relationship, $H = 1.42 dt^{1.44}$ (Fig. 6b, solid black line), by performing a regression using the sediment thicknesses from our successful inversions and the available VoiLA refraction results, where H is sediment thickness in kilometres and dt is mean observed *Ps* delay time in seconds. We also use the initial estimates when thinner than 1 km to fix the beginning portion of the curve to Ruan *et al.* (2014), as they state that their relationship was successful for sediment thickness <1 km. For thicknesses >∼3 km, the curve of our new relationship diverges from the curve assumed from the relationships of Nafe & Drake (1957), Ruan *et al.* (2014), and Bell *et al.* (2015b) (eqs 2 and 3) with smaller thickness predicted for a given delay time. This suggests that thicker sediment packages and/or the thicker sediment packages in particular in the Lesser Antilles require greater V_P/V_S ratios than those implied by eqs (2) and (3). Overall, the new relationship extends the sediment thickness relationship proposed by Ruan *et al.* (2014) and Bell *et al.* (2015b) to thicknesses >10 km (Fig. 6b).

5 CONCLUSIONS

Here we use *Ps* delay times from the crust–sediment conversion of teleseismic earthquake arrivals to estimate the seafloor sediment thickness beneath OBSs of the VoiLA project across the Lesser Antilles, and attempt to synthetically fit the observed daughter-parent amplitude ratios to validate the estimated structure. Average measured delay times range from 0.20 ± 0.06 to 3.55 ± 0.70 s, which generally increase towards the South American continent to the south. The range of initially equated sediment thicknesses beneath OBSs that we successfully synthetically model with a simple single-layered sediment and single-layered crust is 0.43 ± 0.45 to 5.49 ± 3.23 km. Additional layers in the sediment and a variable thickness crust are necessary to synthetically model other OBSs, which we achieve by performing an inversion over a double-layered sediment and single-layered crust, and manually fitting multiple layers interpreted by the VoiLA refraction seismic experiment. The inversions that generate a fit to the observed delay times and amplitude ratios converge on new sediment thicknesses that range from 1.75 km (CR: 1.45–2.02 km) to 7.93 km (CR: 6.32–11.05 km) over different features in the subduction zone. Based on our new inversion sediment thicknesses, VoiLA refraction estimates, and a selection of OBSs that exhibit initial estimates less than 1 km thick, we propose a new delay time–sediment thickness relationship for the Lesser Antilles that may be of use in other thickly sedimented island arc settings.

REFERENCES

Agius, M.R., Harmon, N., Rychert, C.A., Tharimena, S. & Kendall, J.M., 2018. Sediment Characterization at the Equatorial Mid-Atlantic Ridge From P-to-S Teleseismic Phase Conversions Recorded on the PI-LAB Experiment, *Geophys. Res. Lett.,* **45,** 12244–12252.

Aitken, T., Mann, P., Escalona, A. & Christeson, G.L., 2011. Evolution of the Grenada and Tobago basins and implications for arc migration, *Mar. Pet. Geol.,* **28,** 235–258.

Alibés, B., Canals, M., Alonso, B., Lebreiro, S.M. & Weaver, P.P.E., 1996. Quantification of neogene and quaternary sediment input to the Madeira Abyssal Plain, *Geogaceta,* **20,** 394–397.

Allen, R.W., Collier, J.S., Stewart, A.G., Henstock, T., Goes, S. & Rietbrock, A., The VoiLA Team, 2019. The role of arc migration in the development of the Lesser Antilles: a new tectonic model for the Cenozoic evolution of the eastern Caribbean, *Geology,* **47,** 891–895.

Amante, C. & Eakins, B.W., 2009. ETOPO1 1 arc-minute global relief model: procedures, data sources and analysis, NOAA Tech. Memo. NESDIS NGDC-24. Natl. Geophys. Data Center, NOAA.

Bell, S.W., Forsyth, D.W. & Ruan, Y., 2015a. Removing noise from the vertical component records of ocean-bottom seismometers: results from year one of the cascadia initiative, *Bull. seism. Soc. Am.,* **105,** 300–313.

Bell, S.W., Ruan, Y. & Forsyth, D.W., 2015b. Shear velocity structure of abyssal plain sediments in Cascadia, *Seismol. Res. Lett.,* **86,** 1247–1252.

Bird, D.E., Hall, S.A., Casey, J.F. & Millegan, P.S., 1999. Chapter 15 tectonic evolution of the grenada basin, *Sediment. Basins World,* **4,** 403–416.

Bird, P., 2003. An updated digital model of plate boundaries, *Geochem., Geophys. Geosyst.,* **4,** doi:10.1029/2001GC000252.

Bouysse, P., 1988. Opening of the Grenada back-arc Basin and evolution of the Caribbean plate during the Mesozoic and early Paleogene, *Tectonophysics,* **149,** 121–143.

Boynton, C.H., Westbrook, G.K., Bott, M.H.P. & Long, R.E., 1979. Seismic refraction investigation of crustal structure beneath the lesser-antilles Island Arc, *Geophys. J. R. astr. Soc.,* **58,** 371–393.

Christeson, G.L., Mann, P., Escalona, A. & Aitken, T.J., 2008. Crustal structure of the Caribbean-Northeastern South America arc-continent collision zone, *J. geophys. Res.,* **113,** 1–19.

Crawford, W.C. & Webb, S.C., 2000. Identifying and removing tilt noise from low frequency LT0.1Hz seafloor vertical seismic data, *Bull. seism. Soc. Am.,* **90,** 952–963.

Doran, A.K. & Laske, G., 2017. Ocean-bottom seismometer instrument orientations via automated Rayleigh-wave arrival-angle measurements, *Bull. seism. Soc. Am.,* **107,** 691–708.

Hamilton, E.L., 1979. Vp / Vs and Poisson's ratios in marine sediments and rocks, *J. acoust. Soc. Am.,* **66,** 1093–1101.

Harmon, N., Forsyth, D.W., Lamm, R. & Webb, S.C., 2007. P and S wave delays beneath intraplate volcanic ridges and gravity lineations near the East Pacific Rise, *J. geophys. Res.,* **112,** 1–12.

Laske, G., Masters, G., Ma, Z. & Pasyanos, M., 2013. Update on CRUST1. 0—a 1-degree global model of Earth's crust, *EGU Gen. Assem .,* Vienna, Austria. Retrieved from http://igppweb.ucsd.edu/~gabi/rem.html

Leahy, G.M., Collins, J.A., Wolfe, C.J., Laske, G. & Solomon, S.C., 2010. Underplating of the Hawaiian swell: evidence from teleseismic receiver functions, *Geophys. J. Int.,* **183,** 313–329.

Mann, P., 1999. Chapter 1 Caribbean sedimentary basins: classification and tectonic setting from Jurassic to present, *Sediment. Basins World,* **4,** 3–31.

Mascle, A., Cazes, M. & Quellec, P. Le., 1985. Structure des marges et bassins caraïbes: une revue, *Géodynamique des caraïbes,* Symposium, 1–20.

Müller, G., 1985. The reflectivity method: a tutorial, *J. Geophys.,* **58,** 153–174.

Nafe, J.E. & Drake, C.L., 1957. Variation with depth in shallow and deep water marine sediments of porosity, density and the velocities of compressional and shear waves, *Geophysics,* **22,** 523–552.

Picard, M., Schneider, J.-L. & Boudon, G., 2006. Contrasting sedimentary processes along a convergent margin: the lesser Antilles arc system, *Geo-Marine Lett.,* **26,** 397–410.

Ruan, Y., Forsyth, D.W. & Bell, S.W., 2014. Marine sediment shear velocity structure from the ratio of displacement to pressure of Rayleigh waves at seafloor, *J. geophys. Res.,* **119,** 6357–6371.

Rychert, C.A., Harmon, N. & Tharimena, S., 2018. Scattered wave imaging of the oceanic plate in Cascadia, *Sci. Adv.,* **4,** eaao1908, doi:10.1126/sciadv.aao1908.

Rychert, C.A., Rondenay, S. & Fischer, K.M., 2007. P-to-S and S-to-P imaging of a sharp lithosphere-asthenosphere boundary beneath eastern North America, *J. geophys. Res.,* **112,** 1–21.

Shearer, P.M. & Orcutt, J.A., 1987. Surface and near-surface effects on seismic waves—theory and borehole seismometer results, *Bull. seism. Soc. Am.,* **77,** 1168–1196.

Sigurdsson, H., Sparks, R.S.J., Carey, S.N. & Huang, T.C., 1980. Volcanogenic sedimentation in the lesser Antilles Arc, *J. Geol.,* **88,** 523–540.

Speed, R.C., 1993. *Southern Lesser Antilles Arc Platform: Pre-Late Miocene Stratigraphy, Structure, and Tectonic Evolution,* Geological Society of America.

Straume, E.O. *et al.*, 2019. GlobSed: updated total sediment thickness in the World's Oceans, *Geochem., Geophys. Geosyst.,* **20,** 1756–1772.

Udintsev, G.B.(ed.), 1994. *International Geological-Geophysical Atlas of the Atlantic Ocean.* Schweizerbart Science Publishers.

Waltz, R.A., Morales, J.L., Nocedal, J. & Orban, D., 2006. An interior algorithm for nonlinear optimization that combines line search and trust region steps, *Math. Prog., A,* **107,** 391–408.

Wessel, P., Smith, W.H.F., Scharroo, R., Luis, J. & Wobbe, F., 2013. Generic mapping tools: improved version released, *EOS, Trans. (Washington. DC).,* **94,** 409–410.

Zelt, C.A. & Smith, R.B., 1992. Seismic traveltime inversion for 2-D crustal velocity structure, *Geophys. J. Int.,* **108,** 16–34.